Combination of lonidamine with devimistat induces synergistic antitumor effects in lung cancer via multifaceted disruption of cellular energy metabolism

XINHE BAI[1,2*], YONGFENG YANG[1,2*], YULING LUO[1], PEI JING[1,2], XIA HONG[1,2], YAQIN ZOU[1,2], YAN DAI[1,2], XUPING YANG[1,2], MEILING ZHOU[1,2], HAN XIAO[1,2], YILAN HUANG[1,2], SHIWEI GUO[1,2] and QINGZE FAN[1,2]

[1]Department of Pharmacy, Affiliated Hospital, Southwest Medical University, Luzhou, Sichuan 646000, P.R. China;
[2]Department of Clinical Pharmacy, School of Pharmacy, Southwest Medical University, Luzhou, Sichuan 646000, P.R. China

Received February 12, 2026; Accepted August 6, 2026

DOI: 10.3892/or.2026.9184

Abstract. Disrupting energy metabolic pathways has emerged as a promising strategy for cancer therapy including non-small cell lung cancer (NSCLC). However, the ultimate anticancer effects have not been satisfactory. This is likely because cellular energy metabolism encompasses multiple processes and pathways, and tumor cells can flexibly regulate these processes and pathways to adapt to external disturbances and changes in the microenvironment in order to maintain their growth and proliferation. As a result, current strategies which only target certain aspects of energy metabolism have not achieved commendable results. In the present study, two inhibitors lonidamine and devimistat, each with their own limitations, were combined to treat A549 NSCLC by synergistically interfering with the main aspects of cellular energy metabolism including glycolysis, the tricarboxylic acid cycle and oxidative phosphorylation. The synergistic potency was examined *in vitro* and *in vivo* including cytotoxicity, optimal combination doses, colony formation, mitochondrial function, adenosine triphosphate (ATP) and reactive oxygen species (ROS) production, apoptosis and pharmacodynamics in a xenograft mouse model. Moreover, characteristic metabolite levels were measured to elucidate the effects of combination treatment on cellular energy metabolism. The results showed that this combination therapy could synergistically inhibit tumor growth *in vitro* and *in vivo*. Furthermore, combining these two metabolic inhibitors could induce the production of ROS, reduce the generation of ATP, impair mitochondrial morphology and function, and ultimately activate apoptosis in tumor cells through metabolic regulation, facilitating antitumor treatment. The findings underscore the necessity and effectiveness of targeting tumor energy metabolism for lung cancer therapy, providing reliable evidence that metabolic therapies can effectively participate in cancer treatment.

Correspondence to: Dr Qingze Fan or Professor Shiwei Guo, Department of Pharmacy, Affiliated Hospital, Southwest Medical University, 25 Taiping Street, Jiangyang, Luzhou, Sichuan 646000, P.R. China
E-mail: qingzefan017@swmu.edu.cn
E-mail: guoshiwei081@swmu.edu.cn

*Contributed equally

Key words: non-small cell lung cancer, devimistat, lonidamine, glycolysis, tricarboxylic acid cycle, oxidative phosphorylation, combination therapy

Introduction

Cancer is a notable public health issue worldwide, among which lung cancer (LC) represents the most commonly diagnosed cancer and the leading cause of death (1). Traditionally, LC is classified into two main types: i) Non-small cell LC (NSCLC); and ii) small cell LC, with the former accounting for ~85% of cases (2). Traditional treatment modalities for NSCLC, including surgical treatment, chemotherapy and radiotherapy, have yet to fulfill the clinical demands. This underscores the necessity for ongoing research to develop novel therapeutic approaches (3). Tumors, including those present in LC, are characterized by the rapid growth and proliferation of cancer cells, which requires a notable amount of adenosine triphosphate (ATP) as an energy source and a substantial supply of metabolic intermediates for biosynthesis demands. Glucose metabolism including glycolysis, the tricarboxylic acid (TCA) cycle and oxidative phosphorylation (OXPHOS) within the mitochondria, are the main sources of cellular ATP (4). By relying on the altered glycolysis and mitochondrial function, tumor cells acquire metabolic advantages over normal cells for their rapid growth and proliferation. Therefore, targeting tumor metabolic pathways is a potential effective therapeutic strategy (5), or possibly a valuable adjuvant treatment to radio- and chemotherapy (6,7).

Lonidamine (LND), an indole alkaloid, originally explored as a male contraceptive agent for its spermatogenesis-inhibiting properties, has now been acknowledged to exert regulatory effects on tumor metabolism (8,9). LND exerts its antitumor effects mainly through inhibiting key glycolysis enzymes such as hexokinase II and concurrently interfering

with mitochondrial complex I/II to impair OXPHOS (10,11). However, clinical trial results for LND in stages II and III of LC have indicated that its effectiveness is limited and reversible when used alone due to low efficacy *in vivo*, toxicity, resistance and high dosage (12). Consequently, researchers have explored the combination therapies to improve the efficacy and reduce the toxicity of LND. For example, LND was combined with the clinically used DNA alkylating drug nimustine to enhance the antitumor effects in LC cells A549 and H1299 (13). LND was found to exert a chemosensitizer effect by inhibiting energy metabolism, disrupting redox homeostasis and downregulating the expression of DNA repair protein, thereby enhancing the chemotherapeutic efficacy of nimustine. Similarly, combining LND with apigenin, a flavonoid compound present in various fruits and vegetables, could disrupt NAD^+ metabolism, promote apoptosis, inhibit cell migration and synergistically induce antitumor effects in colon cancer cells (14). In another study, the combination of LND and radiotherapy synergistically inhibited tumor growth without any obvious side effects to normal tissues as LND could suppress the repair ability of radiation-induced potentially lethal damage, which is an energy dependent process (15). Moreover, in a recent study, LND was combined with a multifunctional photosensitizer, which could notably enhance the efficacy of photodynamic and photothermal therapy by inhibiting intracellular energy metabolism and downregulating the expression of heat shock protein 90 (16). Collectively, these studies suggest that LND-based combination treatment can potentiate antitumor effects in chemotherapy, radiotherapy, photodynamic therapy and numerous other therapies through disrupting energy metabolism.

However, LND-based combination treatment with another metabolic blocker has not been thoroughly explored for tumor therapy. Apart from glycolysis and OXPHOS which can be disrupted by LND, the TCA cycle is also a core participant of cellular energy metabolism (17,18). In recent years, the TCA cycle has been confirmed to play an indispensable role in maintaining mitochondrial function in most tumors, including NSCLC (19,20). In addition, the TCA cycle mainly uses pyruvic acid produced by glycolysis as a substrate, and it can also be nourished by products from other metabolic pathways such as glutamine metabolism and fatty acid oxidation (21,22). Therefore, it is hypothesized that combining LND with TCA cycle inhibitors to simultaneously interfere with glycolysis, OXPHOS and TCA cycle can more potently disrupt energy metabolism, thereby developing an efficient antitumor strategy.

In the past several decades, numerous researchers have studied various inhibitors targeting the TCA cycle, among which devimistat (CPI-613) has been extensively reported (23-25). CPI-613 is a lipoic acid derivative that effectively inhibits two key enzymes of the TCA cycle: i) Pyruvate dehydrogenase (PDH); and ii) α-ketoglutarate dehydrogenase (α-KGDH) (26,27). Numerous studies have found that CPI-613 can interrupt the supply of ATP from mitochondrial respiration by inhibiting the TCA cycle, demonstrating its potential in cancer therapy (28,29). However, in practical clinical trials, the efficacy of CPI-613 monotherapy was limited (30). As aforementioned, both LND and CPI-613 have notably limited antitumor efficacy when used alone for the inhibition of energy metabolism. Therefore, it is worthwhile to explore the combining antitumor effects of LND and CPI-613, which suppress multiple metabolic pathways and inhibit different metabolic targets.

In the present study, the combination of CPI-613 and LND was applied in A549 NSCLC cells to investigate the synergistic inhibition effects *in vitro* and *in vivo*. The mechanism of combination therapy was assessed by evaluating cellular cytotoxicity, ATP generation and cell death. In addition, major metabolites in metabolic pathways were detected to find their combined influence on energy metabolism.

Materials and methods

Cell lines. NSCLC cell lines A549, H1975, PC9 and HCC827 were purchased from the National Collection of Authenticated Cell Cultures. The cells were cultured with Dulbecco's Modified Eagle Medium (Shanghai VivaCell Biosciences, Ltd.) containing 10% fetal bovine serum (Shanghai VivaCell Biosciences, Ltd.) and 1% penicillin-streptomycin complex (Shanghai VivaCell Biosciences, Ltd.) in a humidified incubator with 5% CO_2 at 37˚C.

Animals. A total of 20 specific pathogen-free male BALB/c nude mice (Beijing Huafukang Biotechnology Co., Ltd., China), aged 4-6 weeks, and weighing 16-19 g were housed under controlled environmental conditions with a 12/12-h light/dark cycle at 20-26˚C and provided with sterilized food and water *ad libitum*. *In vivo* animal experiments were conducted following approval by the Instructional Animal Care and Use Committee of Southwest Medical University (Luzhou, China; approval no. 20210223-079), all procedures adhered to the National Research Council's Guide for the Care and Use of Laboratory Animals, and authors complied with the IACUC guidelines.

Evaluation of cell proliferation. A MTT assay was used to examine the cytotoxic effects of specific drugs on A549 cells. A total of $3x10^3$ cells were inoculated in 96-well plates, and treated with LND (purity, >99%; Meryer (Shanghai) Chemical Technology Co., Ltd.), CPI-613 (purity, >98%; Bide Pharmatech Co., Ltd.) or a combination of both drugs at different concentrations for 24, 48 or 72 h. After which, 100 μl pre-diluted MTT (Beijing Solarbio Science & Technology, Co., Ltd.; 0.5 mg/ml) was added to each well, and the incubation was continued for 4 h. Finally, 110 μl DMSO was added to each well after the solution with MTT was aspirated, and the absorbance of the solution was determined by a microplate reader (Bio-Tek, Inc.) at 490 nm. The measured absorbance is the response to the cell viability rate.

Analysis of the synergistic antitumor effect by SynergyFinder and CompuSyn. A total of $3x10^3$ cells A549 cells were seeded in 96-well plates and left to adhere overnight. After that, the cells were treated with fresh medium containing LND, CPI-613 or a combination of LND and CPI-613 at 37˚C for 72 h (n=5). Subsequently, cell viability was assessed using the MTT assay.

The effects of combining LND and CPI-613 were analyzed by CompuSyn software (version 1.0 by Ting-Chao Chou and

Nick Martin) (31). This method evaluates drug combinations based on the median-effect equation and calculates the combination index (CI) at all investigated doses or effect levels. Specifically, CI>1 indicates antagonism between the two agents, CI=1 indicates additive effect and CI<1 indicates synergism.

Moreover, the obtained cell viability data were input into SynergyFinder (https://synergyfinder.fimm.fi), which utilized the zero-interaction potency (ZIP) model to analyze the interaction between the two drugs. Based on the synergy scores derived from the dose-response curves provided by the software, it was determined whether the combination exhibited synergistic, additive or antagonistic effects. Specifically, a ZIP score <-10 indicated potential antagonism between the two agents, a ZIP score between -10 and 10 suggested an additive effect, and a ZIP score >10 indicated the possibility of synergism between the two drugs.

Colony formation assay. Colony formation assays were conducted to investigate the inhibitory effects of LND in combination with CPI-613 on the proliferation of tumor cells. A total of 300 A549 cells were seeded into each well of a six-well plate and incubated at 37˚C for 24 h. Subsequently, the cells were treated with different drugs (LND at 150 μM, CPI-613 at 150 μM or LND + CPI-613 at 150 μM each) and further cultured for 1-2 weeks. After that, the cells were fixed with 4% paraformaldehyde at room temperature for 20 min and stained with 0.5% crystal violet at room temperature for 10 min. The wells were rinsed twice with PBS and allowed to dry. Finally, images of the cell colony area were captured and colonies containing >50 cells were counted and analyzed using the Cytation 5 High-Throughput Cell Imaging System (Bio-Tek, Inc.).

Real-time imaging of living cells. Cellular changes were monitored in real-time using the Incucyte SX5 (Sartorius AG). A total of $3.5x10^3$ cells were seeded in a 96-well plate. Once the cells were fully adhered, fresh medium (control group) or fresh medium containing LND (150 μM), CPI-613 (150 μM) or a mixture of both drugs (LND and CPI-613; 150 μM each) were added for incubation at 37˚C for 72 h; each group included six replicate wells. After addition of the drugs, the plate was placed under a live cell microscope system of Incucyte SX5 to capture four images from each well every 6 h for 72 h. Subsequently, the collected images were quantitatively analyzed using the Incucyte S3 analysis system EssenBioscience (Sartorius AG) to calculate the cellular viability among different groups.

In vivo antitumor efficacy. A549 LC cells ($4x10^6$) were inoculated subcutaneously into the right flank of each BALB/c nude mouse to establish a xenograft model. When the tumor volume approached ~100 mm^3, the mice were randomly divided into four groups: i) Ctrl group; ii) LND group; iii) CPI-613 group; and iv) LND + CPI-613 group. Every four days, the mice received intratumoral injections of LND at a dose of 40 mg/kg and/or CPI-613 at a dose of 48 mg/kg. Mouse body weight was recorded, and tumor volume were calculated using the following formula: Tumor volume (mm^3)=tumor length x tumor $width^2/2$. The drug was administered every four days for eight consecutive doses, and detection of changes in tumor volume was continued after discontinuation of the drug. On day 36, mice were injected intraperitoneally with a lethal dose of sodium pentobarbital (150 mg/kg), and cervical dislocation was carried out to confirm the death of the mice. After that, mouse blood samples were collected for biochemical analysis to evaluate the adverse effects of the drugs on hepatic and renal functions, and heart, liver, spleen, lung, kidney and tumor tissues were harvested for pathological analysis. The experimental protocol was approved by the Instructional Animal Care and Use Committee of Southwest Medical University (Luzhou, China; approval no. 20210223-079), and all procedures adhered to the National Research Council's Guide for the Care and Use of Laboratory Animals. The tumor burden did not exceed a diameter of 2.0 cm at their widest point.

Immunohistochemistry. Immunohistochemistry was performed on 3-μm-thick paraffin-embedded tumor tissue sections. After deparaffinization in xylene and rehydration of tissue sections through a descending ethanol series (100, 95, 90, 80%, 2 min each) to distilled water, antigen retrieval was performed using the microwave method, followed by blocking non-specific antigens with 5% normal goat serum (Beijing Zhongshan Golden Bridge Biotechnology Co., Ltd.). After that, the primary antibody (Ki-67; cat. no. GB111499; 1:1,000; Wuhan Servicebio Technology Co., Ltd.) was added for incubation overnight at 4˚C, and after washing with PBS, the secondary antibody of horseradish peroxidase (HRP)-conjugated Goat Anti-Rabbit IgG (H+L) (1:1,000; cat. no. 111-035-003; Jackson ImmunoResearch Laboratories, Inc.) was applied for incubation at 37˚C for 60 min. DAB (Wuhan Servicebio Technology Co., Ltd.) was used for chromogenic detection, and the nuclei were counterstained with hematoxylin. Finally, the sections were dehydrated, cleared and mounted. Observations were made under a light microscope.

Targeted metabolomics assay. The gas chromatography-mass spectrometry (GC-MS) targeted metabolomics assay was conducted similarly to a previous method with some modifications (32).

GC-MS metabolite extraction. A549 cells were treated with LND (150 μM), CPI-613 (150 μM) or a mixture of both drugs (LND and CPI-613; 150 μM each) at 37˚C for 48 h. The cells were rinsed with pre-cooled PBS on dry ice after the removal of the culture medium. After that, 80% methanol containing 2.5 μg/ml myristic d-27 acid (Thermo Fisher Scientific, Inc.) was added, and the cells were quenched at -80˚C for 30 min. The cells were collected with a scraper, the samples were shaken at 4˚C, 200 x g for 10 min and sonicated for 10 min at 4˚C. After centrifugation at 4˚C, 16,200 x g for 20 min, the supernatant was aspirated and dried in a centrifugal concentrator, and 100 μl 80% methanol was added. Finally, the samples were subjected to shaking, sonication, centrifugal concentration and drying, and finally stored at -80˚C.

Sample derivatization. The samples were removed from -80˚C storage, and 45 μl methoxy-amine hydrochloride pyridine (MilliporeSigma; Merck KGaA; 20 mg/ml) was added and incubated in a thermal shaker at 37˚C with shaking at 500 rpm in the dark for 120 min. After which, 45 μl MSTFA (with 1% TMCS; Agilent Technologies, Inc.) was added and

mixed evenly. The samples were incubated in a metal bath at 37˚C and 500 rpm in the dark for 90 min. Finally, the supernatant was centrifuged and transferred into glass sample injection vials.

GC-MS. GC-MS analysis was performed on a GC system coupled to a mass spectrometer (Agilent 8890/LECO Pegasus BT GC-TOF MS). A Rxi-5ms capillary column (30 m x 250 μm x 0.25 μm) was used to separate the derivatized sample. The injection volume was 1 μl, with helium used as the carrier gas at a flow rate of 1 ml/min. The temperature of the injector was 250˚C, whereas the GC temperature program was as follows: 80˚C (2 min), 12˚C/min to 176˚C (0 min), 8˚C/min to 196˚C (1 min) and 12˚C/min to 300˚C (10 min). The temperatures of the transfer line and ion source were 280 and 250˚C, respectively. The mass spectrometry original data were acquired with electron impact ionization (70 eV) and the spectra were recorded within the mass range of 50-550 m/z.

PDH activity detection. PDH activity in A549 cells was detected by the PDH Activity Assay Kit (Solarbio Science & Technology, Co., Ltd.) according to manufacturer's instructions. In total, three replicates of cells were collected and washed with cold PBS after different treatment with LND, CPI-613 or their combination. Meanwhile, after cell counting, the cells were sonicated in an ice bath, and the supernatant was centrifuged at 11,000 x g for 10 min at 4˚C. Then 50 μl of supernatant and 900 μl of the working solution were added to the quartz cuvette, and the OD value at 605 nm was determined at 10 sec and 1 min 10 sec. PDH activity levels were normalized to the cell number.

α-KGDH activity detection. α-KGDH activity in A549 cells was detected by the α-KGDH Activity Assay Kit (Solarbio Science & Technology, Co., Ltd.) according to manufacturer's instructions. In total, three replicates of cells were collected and washed with cold PBS after different treatment with LND, CPI-613 or their combination. Meanwhile, after cell counting, 1 ml of Reagent 1 and 10 μl of Reagent 2 were added and cells were sonicated in an ice bath, and the supernatant was centrifuged at 11,000 x g for 10 min at 4˚C. Then 60 μl of supernatant, 40 μl of Reagent 8 and 900 μl of the working solution were added to the quartz cuvette, and the OD value at 340 nm was determined at 10 sec and 2 min 10 sec. α-KGDH activity levels were normalized to the cell number.

Reactive oxygen species (ROS) assay. The intracellular levels of ROS were measured using the DCFH-DA fluorescent probe method and ROS Assay Kit (Beyotime Institute of Biotechnology). DCFH-DA can freely permeate the cell membrane and be hydrolyzed by esterase to DCFH. Intracellular ROS can further oxidize DCFH to produce the fluorescent compound DCF. Therefore, the fluorescence intensity of DCF detected in the cells can reflect the intracellular ROS levels. In brief, A549 cells ($3x10^5$) were seeded in six-well plates and treated with fresh medium containing LND (150 μM), CPI-613 (150 μM) or a combination of LND (150 μM) and CPI-613 (150 μM) at 37˚C for 24 h. After incubation, the diluted DCFH-DA fluorescent probe was added and incubated at 37˚C for 20 min. The fluorescence intensity of DCF within the cells was assessed using the DMi8 Automated Inverted Fluorescence Microscope (Leica Microsystems GmbH) to detect intracellular ROS levels.

JC-1 analysis for mitochondrial membrane potential (MMP). MMP was assessed using the MMP Assay Kit (Beyotime Institute of Biotechnology). A549 cells were seeded in six-well plates at a density of $3x10^5$ cells/well. After that, cells were treated with fresh medium containing LND (150 μM), CPI-613 (150 μM), or a combination of LND (150 μM) and CPI-613 (150 μM) at 37˚C for 24 h. After washing with PBS, the cells were incubated with 10 μM JC-1 dye at 37˚C in the dark for 20 min. Following incubation, the cells were washed again with PBS to remove unbound JC-1. Fluorescence images were observed using a DMi8 automated inverted fluorescence microscope (Leica Microsystems GmbH) to assess the changes in MMP after different treatments. Data were analyzed using GraphPad Prism 9.0 (Dotmatics) to determine the effects of LND, CPI-613 and their combination on MMP variation, which serves as an indicator of mitochondrial function.

Intracellular ATP levels. Intracellular ATP concentrations were detected using an ATP assay kit (Beyotime Institute of Biotechnology). A total of $3x10^5$ A549 cells were seeded into 6-well plates and treated with fresh medium containing LND (150 μM), CPI-613 (150 μM) and LND (150 μM) + CPI-613 (150 μM) for at 37˚C 72 h. After incubation, ATP content was measured by the ATP Assay Kit following the manufacturer's instructions. As ATP is required in the luciferin-luciferase reaction system to emit bioluminescence, the bioluminescence measured by a luminometer (EnVision 2015; PerkinElmer, Inc.) can be expressed as the amount of ATP.

Malondialdehyde (MDA) assay. A549 cells ($3x10^5$) were seeded into six-well plates and left to adhere overnight. After which, the cells were treated with fresh medium containing LND (150 μM), CPI-613 (150 μM), or a combination of LND (150 μM) and CPI-613 (150 μM) at 37˚C for 24 h. After treatment, the cells were resuspended with PBS and lysed by sonication. MDA levels were quantified using the MDA Assay Kit (Wuhan Servicebio Technology Co., Ltd.) according to the manufacturer's instructions. Briefly, the cell lysate was mixed with the MDA reagent provided in the kit and incubated at 95˚C for 30 min to promote the reaction. After cooling, the solution was centrifuged at 1,000 x g for 10 min at room temperature to remove the residue. The supernatant was transferred to a 96-well plate and the optical density was measured at a specific wavelength (532 nm) using a microplate reader. The level of lipid peroxidation in treated A549 cells was determined by calculating the MDA concentration from a standard curve generated using an established concentration of MDA.

Isolation of mitochondria from A549 cells. After treatment, mitochondria were isolated from A549 cells using an Animal Tissue/Cell Mitochondria Isolation Kit (Wuhan Servicebio Technology Co., Ltd.) following the manufacturer's instructions with minor modifications. Briefly, after treatment with LND, CPI-613, or their combination, ~$5x10^6$ A549 cells were collected and washed twice with ice-cold PBS. Cell pellets

were resuspended in 1 ml of ice-cold mitochondria isolation reagent A, then gently pipetted, homogenized on ice bath for 50 times to disrupt cell membranes. The lysate was centrifuged at 1,000 x g for 10 min at 4˚C to remove nuclei, cell debris and unbroken cells. The supernatant was centrifuged at 12,000 x g for 10 min at 4˚C. The resulting supernatant was collected as the cytosolic fraction, which was subsequently used for cytochrome c detection by western blotting. The pellet was collected and washed twice with mitochondria isolation reagent A 12,000 x g, 10 min, 4˚C). At last, the mitochondrial pellets were collected and used for cytochrome c detection by western blotting.

Western blotting. After treatment, A549 cells or isolated mitochondria were collected and lysed using RIPA solution (Beyotime Institute of Biotechnology) supplemented with PMSF (Beyotime Institute of Biotechnology). Subsequently, the lysate was subjected to centrifugation at 4˚C, 12,000 x g for 10 min to obtain the supernatant. Protein concentration was determined using a BCA assay kit (Beyotime Institute of Biotechnology) according to the manufacturer's instructions. After that, the proteins in the supernatant were separated and detected using western blot analysis. Specifically, 20 μg of protein samples were separated by 10 or 12.5% SDS-PAGE (Oriscience Biotechnology Co., Ltd.) under a constant current and subsequently transferred to a PVDF membrane (MilliporeSigma) at a constant voltage. The membrane was blocked for 15 min using a Protein-Free Rapid Blocking Buffer and washed three times with Tris-buffered saline containing 0.1% Tween 20 (TBST; Shanghai Yuanye Bio-Technology, Co., Ltd.). After that, the membrane was incubated overnight at 4˚C with the following primary antibodies: β-actin rabbit pAb (1:10,000; cat. no. AC006; ABclonal Biotech Co., Ltd.), anti-cleaved poly (ADP-ribose) polymerase (PARP)-1; 1:1,000; cat. no. BML-SA249; Enzo Life Sciences, Inc.), anti-caspase 3 (1:2,000; cat. no. A19654; ABclonal Biotech Co., Ltd.), anti-Bax pAb (1:10,000, cat. no. ER0907; Huabio Co., Ltd.), anti-Bcl-2 mAb (1:10,000, cat. no. ET1702-53; Huabio Co., Ltd), anti-Cytochrome c mAb (1:5,000, cat. no. A4912; Abclonal Biotech Co., Ltd.) and anti-VDAC1 mAb (1:2,000, cat. no. YP-rAb-17947; UpingBio technology Co., Ltd.). After removing the primary antibodies, the membrane was washed three times with TBST. Next, the secondary antibodies of HRP-conjugated Goat Anti-Rabbit IgG (H+L) (1:10,000; cat. no. AS014; ABclonal Biotech Co., Ltd.) were applied and incubated at room temperature for 2 h. Ultimately, the target protein bands were visualized using an ECL substrate (Beyotime Institute of Biotechnology) and imaged with a Syngene G: Box system (Syngene). Quantification was performed using ImageJ software (version 1.54g; National Institutes of Health).

Statistical analysis. Statistical analysis of all experimental data was performed using GraphPad Prism 9.0 (Dotmatics). Data were presented as the mean ± standard deviation. Statistical significance analyses of the experimental data were derived by unpaired Student's t-test or one-way ANOVA test followed by Tukey's or Dunnett's test. $P<0.05$ was considered to indicate a statistically significant difference.

Results

LND and CPI-613 induce antitumor effects on NSCLC cells in vitro. LND and CPI-613 were used to treat NSCLC cell lines (H1975, HCC827, PC9 and A549) for 48 h. For LND treatment, the IC_{50} in H1975, HCC827, PC9 and A549 cells were 741.4, 403.2, >1,000 and 394.3 μM, respectively (Fig. 1A). For CPI-613 treatment, the IC_{50} in H1975, HCC827, PC9 and A549 cells were 299.4, 266.0, 201.3 and 252.8 μM, respectively (Fig. 1B and C). Moreover, in A549 cells, the CI values across all Fa values (ranging from 0 to 1) for LND + CPI-613 treatment were <0.9, suggesting that this combination synergistically inhibited the viability of A549 cells (Fig. 1D). In H1975 cells, CI values were <1 only when Fa was <0.6, indicating that the drug combination showed synergistic antitumor effects at lower inhibition levels, but additive or antagonistic effects at higher inhibition levels. Moreover, for HCC827 and PC9 cells, CI values were >1 for most Fa values, indicating that the interaction was largely antagonistic. As A549 cells showed the highest sensitivity to both LND and CPI-613 (lowest IC_{50} value) and a synergistic antitumor effect upon combination treatment, A549 cells were selected as the most suitable NSCLC cells for subsequent investigation.

Validation and optimal dosage of LND + CPI-613 for synergistic inhibition of the proliferation and survival on A549 NSCLC cells by combination treatment. MTT cytotoxicity assays were further performed on A549 cells to investigate IC_{50} values at different times. The results showed that the IC_{50} values for both LND (Fig. S1A) and CPI-613 (Fig. S1B) were time-dependent on A549 cells, with both IC_{50} values decreasing with prolonged drug exposure. The synergistic effect of both drugs on A549 cells was further analyzed by SynergyFinder. The full dose-response matrices were shown in Fig. S2A and B. The ZIP synergy score was calculated as 12.708 with a 95% confidence interval of 0.95 via SynergyFinder 3.0, indicating a high level of synergy between LND and CPI-613 on A549 cells (a ZIP score >10 indicates notable synergy and the maximum synergistic area is represented by the white rectangle; Fig. 2A, Table SI). The best synergistic effect was observed with LND concentrations 100-300 μM combined with CPI-613 concentrations 100-250 μM. Furthermore, the combination of CPI-613 at 150 μM with LND at the mol ratio of ~1:1 (150:150 μM) encompassed the region of highest synergy and significantly inhibited A549 cell proliferation and markedly induced cell death. Thus, the concentration of 150 μM for both LND and CPI-613 at the mol ratio of 1:1 was selected as the best combined concentration for subsequent experiments.

To improve validation of the effects of LND and CPI-613 on A549 cell proliferation and cytotoxicity during combination treatment, colony-forming assays and real-time dynamic live cell imaging analysis (Incucyte SX5; Sartorius AG) were performed. The results of the colony-forming assay demonstrated that the number and area of colonies in the LND and CPI-613 combination treatment group were significantly lower than that in the control group and the monotherapy groups, indicating that the combination treatment significantly inhibited the colony-forming capacity of A549 cells (Figs. 2B and C; and S3). The results of real-time dynamic

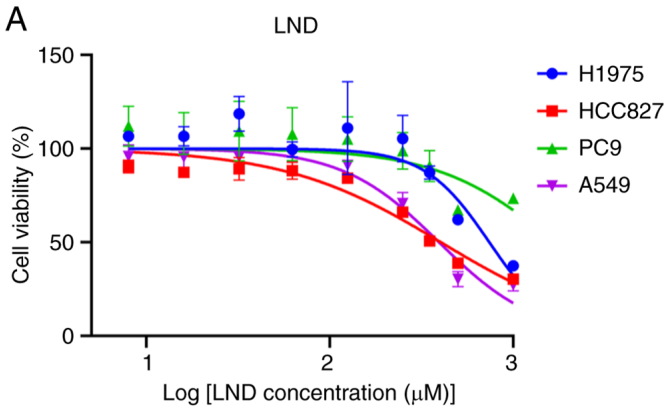

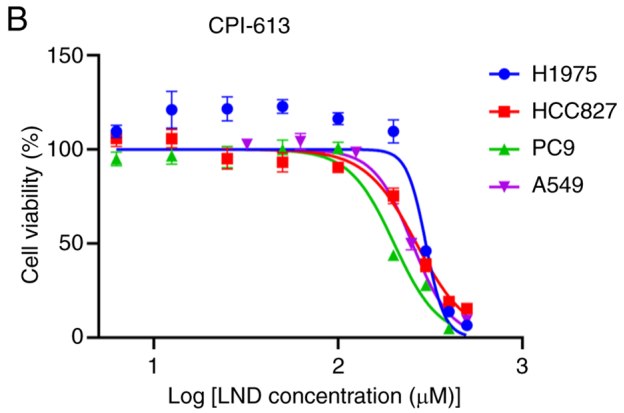

C

Cell lines	IC_{50} (μM)	
	LND	CPI-613
H1975	741.4	299.4
HCC827	403.2	266.0
PC9	> 1000	201.3
A549	394.3	252.8

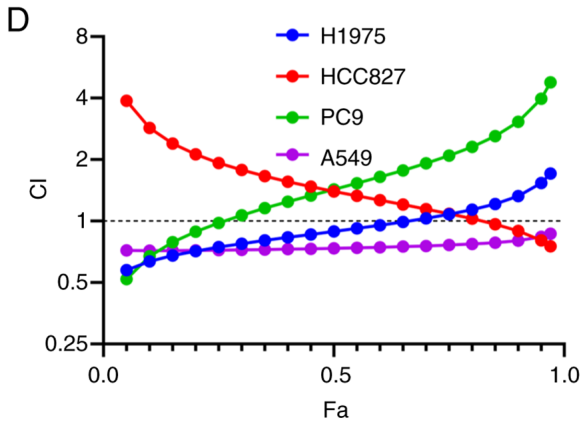

Figure 1. LND and CPI-613 treatment show antitumor effects in NSCLC cells (H1975, HCC827, PC9 and A549) and their combination effects. (A) Dose effect curves of LND in different NSCLC cells (n=6). (B) Dose effect curve of CPI-613 in different NSCLC cells (n=6). (C) IC_{50} for LND and CPI-613 in different NSCLC cells. (D) CI values vs. different Fa values for the combination of LND and CPI-613 in different NSCLC cells. The dashed line in the figure represents a CI value of 1.0. CI, combination index; LND, lonidamine; CPI-613, devimistat; NSCLC, non-small cell lung cancer.

live cell monitoring experiments showed that starting at ~24 h after the combination treatment of LND and CPI-613, the cell morphology and proliferative capacity of A549 cells were markedly different from the other three groups (Fig. 2D). A total of ~24 h after the combination treatment, A549 cells exhibited significantly deteriorated morphology, which was worsened with prolonged exposure. Concurrently, the cell proliferation rate in the combination treatment group was also significantly suppressed, ultimately resulting in a marked decrease in A549 cell proliferative capacity and an increase in cell death (Fig. 2E).

CPI-613 enhances the antitumor effects of LND on A549 cells in vivo. In vitro experimental results indicated that combined treatment with LND and CPI-613 induced a synergistic antitumor effect on A549 cells. To investigate the synergistic effects of the combined treatment *in vivo*, a subcutaneous xenograft tumor model was established in nude mice by implanting A549 cells. A total of two weeks after the implantation of A549 cells, the mice were injected with physiological saline as a control, LND (40 mg/kg) alone, CPI-613 alone (48 mg/kg), and a combination of LND (40 mg/kg) and CPI-613 (48 mg/kg; Fig. 3A). At the end of the experiment, the mice were euthanized, and their blood, vital organs and tumor tissues were collected for subsequent biochemical and pathological analyses. During the drug administration period, changes in body weight (Fig. 3B) and tumor volume (Fig. 3C) were regularly monitored. Notably, both tumor volume (Fig. 3C) and tumor weight (Fig. 3D) in treated mice were significantly diminished compared with the control group. The inhibitory effect of LND combined with CPI-613 treatment group on tumor growth was also clearly observed in isolated tumors (Fig. 3E). Following the histological processing of tumor tissues, H&E staining, TUNEL staining and immunohistochemical analysis for Ki-67 were performed (Fig. 3F). The results revealed that tumor tissues from the LND and CPI-613 combination treatment group exhibited the highest apoptotic rate and the lowest proliferation rate. These findings suggested that combination of LND and CPI-613 significantly enhanced the inhibitory effects on tumor growth *in vivo*.

In vivo safety analysis. The systemic safety profiles of different treatments in mice were evaluated by monitoring changes in body weight and various biochemical indicators, as well as histopathological tissue examination. Throughout the experimental period, all groups of mice exhibited an upward trend in body weight with no significant differences (Fig. 3B). The potential toxicity of drugs on vital organs was also analyzed by H&E staining. H&E staining images revealed no histopathological abnormalities in the vital organs (heart, liver, spleen, lungs and kidneys) of the mice (Fig. 4A). Serum biochemical analysis demonstrated no significant differences in hepatic functional markers (aspartate aminotransferase

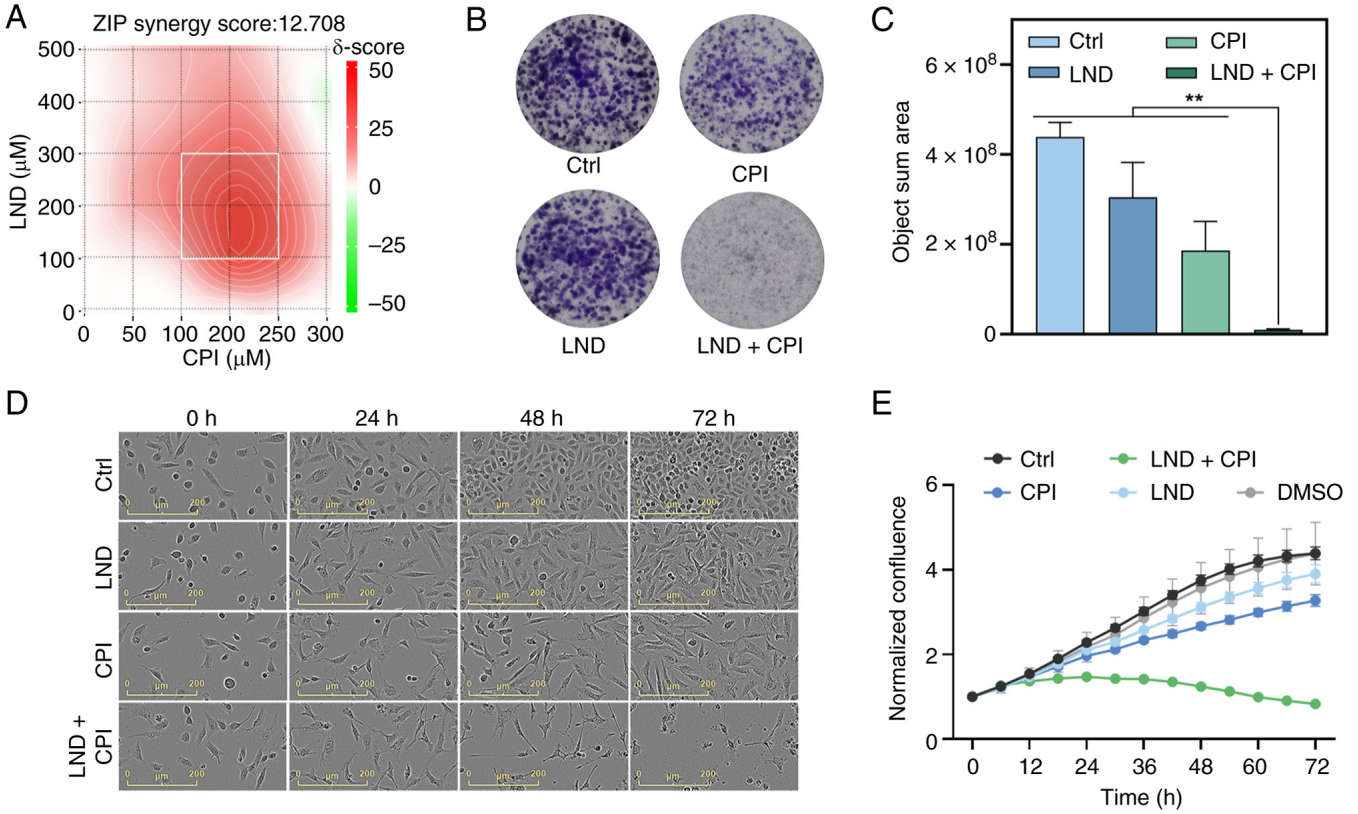

Figure 2. LND combined with CPI-613 inhibits A549 NSCLC cell proliferation and induces cell death. (A) Heatmap of drug combination response (n=5). The cell viability was detected by MTT assay. ZIP Synergy score was calculated using Synergyfinder 3.0 software. A score >10 indicates possible synergy. The red gradient area indicates the strength of drug synergy. The white rectangles indicate the concentration regions with the strongest synergistic effect. (B) Representative images of colony formation in A549 cells after combined treatment and (C) quantitative analysis of the cell colony area across experimental groups (n=3). (D) Real-time imaging of live cells and (E) statistical analysis of cell viability (n=5). **P<0.01. LND, lonidamine; CPI-613, devimistat; NSCLC, non-small cell lung cancer.

and alanine aminotransferase), renal functional parameters (UREA) and lactate dehydrogenase between the combined treatment group and control group (Fig. 4B-E). In summary, these results demonstrated that the combined treatment of LND and CPI-613 was well-tolerated in mice with no obvious toxic side effects, suggesting a favorable safety profile *in vivo*.

Combined LND and CPI-613 treatment inhibits energy metabolism in A549 cells. Considering the metabolic inhibitor attributes of LND and CPI-613, the effect of their combination treatment on cellular energy metabolism was firstly investigated using GC-MS targeted metabolomics technology. It was observed that in the glycolysis process, the combination treatment of LND and CPI-613 reduced the utilization of glucose by the cells, as demonstrated by an increase in the amount of intracellular glucose (Fig. 5A). Meanwhile, the key substances for glycolysis, 1,6-bisphosphofructose (Fig. 5B), 3-phosphoglycerate (Fig. 5C) and phosphoenolpyruvate (Fig. 5D), were significantly inhibited. The notable decrease in the content of pyruvic acid (Fig. 5E) also confirmed this inhibition. These results demonstrated that a stronger decrease of the metabolites involved in glycolysis was observed in the combination treatment group.

In addition, it was observed that mitochondrial function was subjected to stronger suppression during combination treatment with LND and CPI-613. First, the decrease in total intracellular pyruvic acid (Fig. 5E) suggested a reduction in pyruvic acid entering the mitochondria to participate in the TCA cycle. Meanwhile, it could be observed that the production of citrate (Fig. 5F) and α-ketoglutaric acid (Fig. 5G) were significantly inhibited, demonstrating a weakened mitochondrial function within the cells. There was no difference in succinate (Fig. 5H), which was probably due to the compensation effects from alternative metabolic pathways. It was shown that the production of succinate and fumarate were similar between control group and combination group (Fig. 5I), but the malate was significantly inhibited by the combined treatment (Fig. 5J). These results demonstrated that a stronger decrease of the metabolites involved in mitochondrial respiration was also observed in the combination treatment group.

To further confirm that the combined treatment could inhibit glycolysis and mitochondrial respiration, extracellular lactate level and activities of two key enzymes of TCA cycle were detected. As shown in Fig. S4, compared with the control group and LND single treatment group, the combined treatment of LND and CPI-613 revealed a significant reduction in extracellular lactate content. Moreover, activity of PDH, which was a key indicator of the transition efficiency from glycolysis to mitochondrial respiration, was also significantly decreased after combination treatment (Fig. S5). Both results could indicate effective suppression of glycolytic activity in tumor cells. Consistent with the inhibition of mitochondrial respiration,

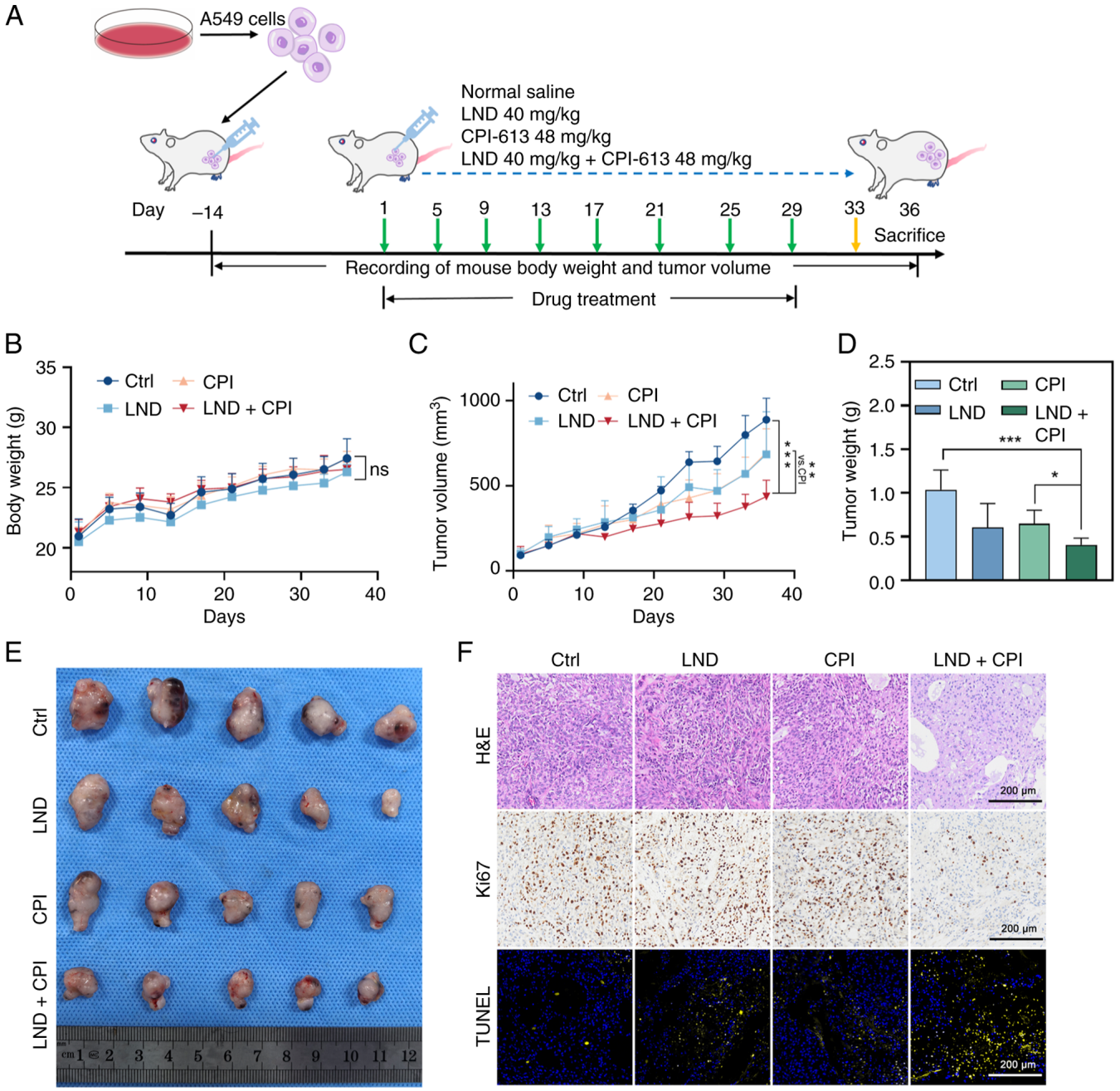

Figure 3. Combination treatment of LND and CPI-613 induces synergistic inhibition of tumor growth *in vivo*. (A) Scheme of tumor transplantation and drug administration to nude mice. (B) Change of body weight and (C) tumor volume with time, and (D) tumor weight at the end of the experiment on day 36 (n=5). (E) Images of solid tumors dissected from animals on day 36 (n=5). (F) Tumor tissue H&E staining, Ki-67 immunohistochemistry and TUNEL analysis. *P<0.05, **P<0.01 and ***P<0.001. ns, no significance; LND, lonidamine; CPI-613, devimistat.

the combined treatment significantly reduced α-KGDH activity compared with the control and LND groups, further confirming that the combined treatment could effectively inhibit mitochondrial respiration in tumor cells (Fig. S5).

Second, the suppression of mitochondrial function is also associated with the inhibition of the respiratory chain, including a blockage of electron transfer and electron leakage, which may result in the formation of ROS (33,34). Thus, the combined effect of LND and CPI-613 on ROS production was determined using DCFH-DA fluorometry. The green fluorescence indicated that the ROS level in the single drug groups was notably weak (Fig. 6A and B). By contrast, combination treatment of LND and CPI-613 induced significantly higher ROS. The electron microscopy images exhibited notable changes in mitochondrial morphology after the combined treatment of LND and CPI-613, primarily characterized by a reduction in mitochondrial volume, increased electron density and disorganization of mitochondrial cristae (Fig. 6C and D). These results indicated that LND combined with CPI-613 treatment could alter the mitochondrial morphology in A549 cells. Moreover, MMP depolarization was observed, with stronger green-fluorescent intensity of JC-1 monomers and weaker red fluorescent intensity of JC-1 aggregates; the monotherapy groups and control groups showed less depolarized MMP

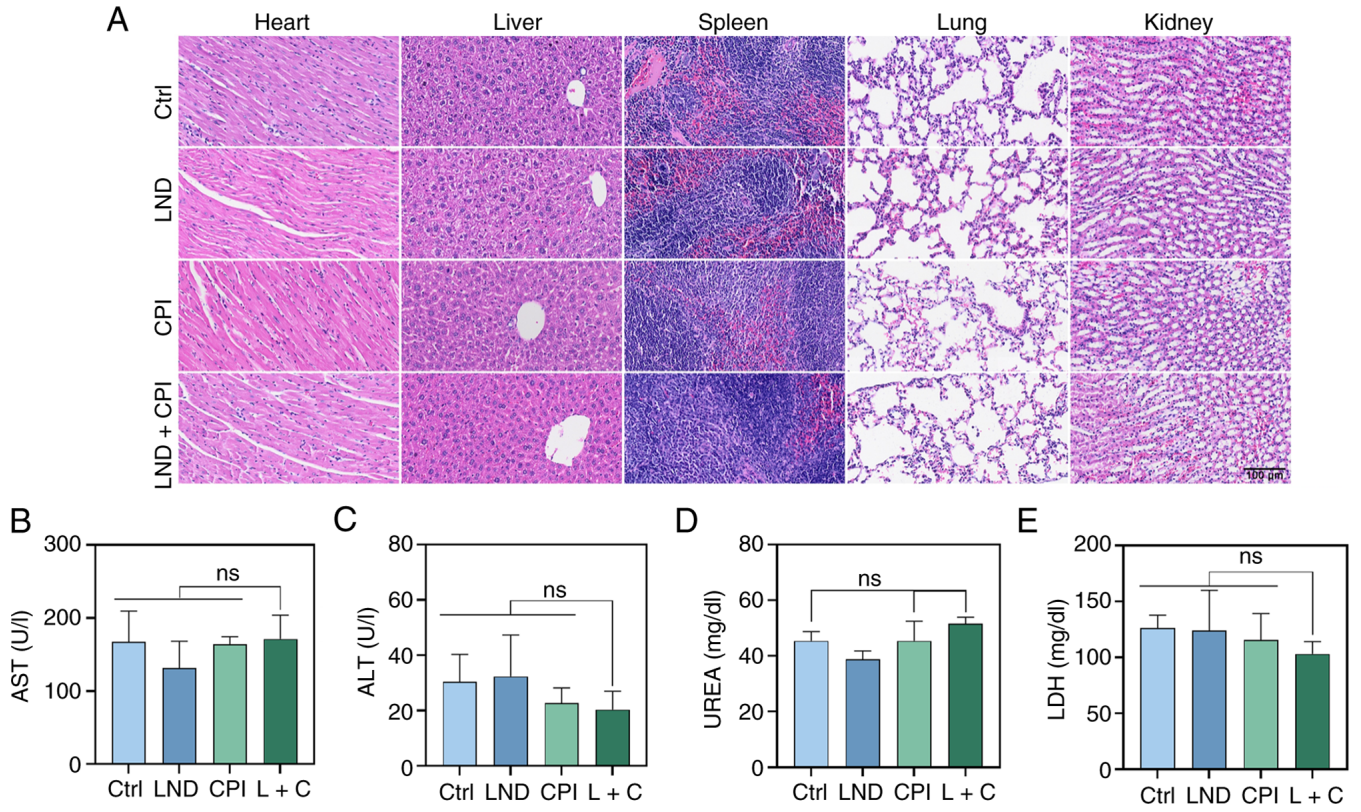

Figure 4. Systemic safety profiles of different treatments in mice. (A) H&E staining of the heart, liver, spleen, lungs and kidneys. (B-E) Biochemical indicators of serum (B) AST, (C) ALT, (D) UREA and (E) LDH (n=5). ns, no significance; AST, aspartate aminotransferase; ALT, alanine aminotransferase; UREA, urea; LDH, lactate dehydrogenase.

(Fig. 6E). Statistical analysis also revealed similar patterns (Fig. 6F). Moreover, the combination treatment significantly upregulated intracellular MDA levels, indicating that the cells were under oxidative stress conditions (Fig. 6G). These results demonstrated that the combination treatment of LND and CPI-613 may be the cause of significant oxidative stress and dysfunction in mitochondria, including structural changes and depolarization of MMP in A549 cells.

As a principal product of cellular energy metabolism, ATP is important in maintaining the cell viability and providing energy for biochemical reactions. Therefore, the changes in ATP content in A549 cells was investigated during LND and CPI-613 combination treatment. At 24 h, both single treatment with LND or CPI could moderately increase ATP levels, whereas the combination treatment showed a slight increase in ATP content. At 48 h, ATP levels remained relatively stable across all groups, with no significant differences between the combination group and either monotherapy or the control group. Notably, the results revealed that after 72 h of combination treatment, the ATP levels in A549 cells were significantly reduced, far exceeding that of other treatment groups (Fig. 6H). This marked decline in ATP levels at 72 h indicates that the combined treatment of LND and CPI-613 could effectively impair glycolysis and mitochondrial function, thereby causing the dysfunction of energy metabolism in tumor cells.

Combined treatment with LND and CPI-613 induces synergistic effects on apoptosis in A549 cells. Considering the notable increase in cell death and dysfunction of cellular energy metabolism after co-incubation of LND and CPI-613, the effect of the combination treatment on inducing cell apoptosis was analyzed by flow cytometry. The results showed that the ratio of apoptotic cells in the LND single-drug group or CPI-613 single-drug group exhibited similar patterns to those of the control group (Fig. 7A). However, the ratio of apoptotic cells in the combined treatment group of LND and CPI-613 (29.04%) was significantly increased, and there were significant differences compared with the control group (3.79%), the LND (4.09%) and CPI-613 (8.83%) single-treatment groups (Fig. 7B). Western blot analysis revealed significant upregulation of apoptotic markers after co-treatment with LND and CPI-613 (Fig. 7C). Specifically, the protein level of Bax was upregulated (Fig. 7D), while Bcl-2 expression was slightly downregulated (Fig. 7E), leading to a pronounced increase in the Bax/Bcl-2 ratio (Fig. 7F). In addition, the levels of cleaved caspase 3 (Fig. 7G) were significantly increased following combination treatment, although the total caspase 3 expression (Fig. 7H) remained unchanged. Moreover, after combination treatment, the levels of cleaved PARP were slightly upregulated (Fig. 7I) and the total PARP was slightly downregulated (Fig. 7J), leading to a pronounced increase in the cleaved PARP/total PARP ratio (Fig. 7K). Furthermore, co-treatment of LND and CPI-613 caused a reduction in cytochrome c content in the mitochondrial fraction, accompanied by an increase in the cytoplasmic fraction (Fig. S6). Mechanistically, impaired cellular energy metabolism promotes the upregulation of pro-apoptotic Bax and the subsequent release of cytochrome c from mitochondria into the cytoplasm. This event initiates

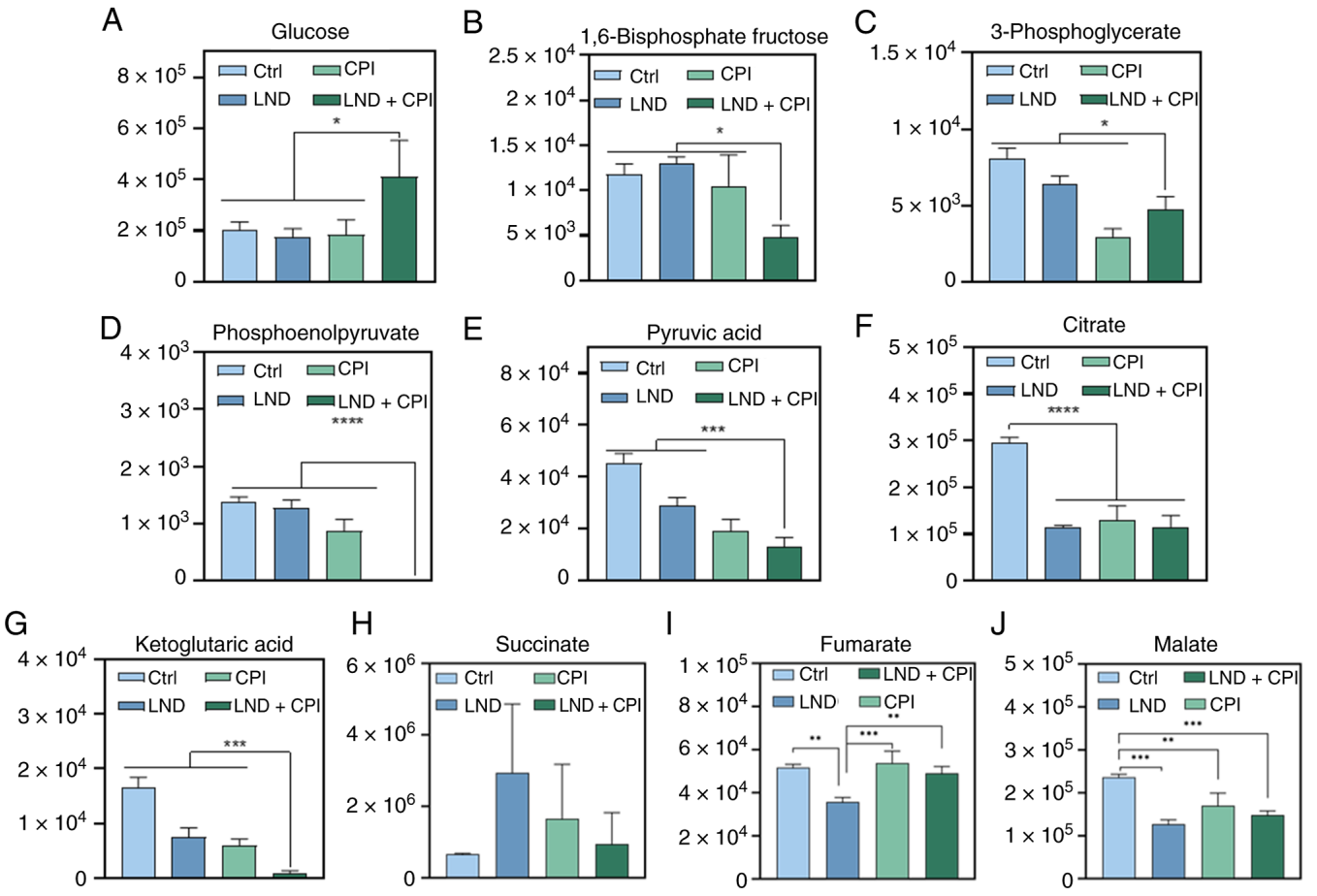

Figure 5. GC-MS-targeted metabolomics assay of different treatments in tumor cells. (A-J) GC-MS analysis of the differences in major metabolites in cellular energy metabolism among the four experimental groups, including (A) glucose, (B) 1,6-bisphosphate fructose, (C) 3-phosphoglycerate, (D) phosphoenolpyruvate, (E) pyruvic acid, (F) citrate, (G) α-ketoglutaric acid, (H) succinate, (I) fumarate and (J) malate. *P<0.05, **P<0.01, ***P<0.001 and ****P<0.0001. GC-MS, gas chromatography-mass spectrometry; LND, lonidamine; CPI-613, devimistat.

the proteolytic cleavage and activation of caspase 3, which in turn catalyzes the cleavage of PARP, resulting in the loss of its DNA repair enzymatic activity and subsequent acceleration of apoptosis.

In summary, combination treatment of the two metabolism inhibitors LND and CPI-613 could efficiently suppress both glycolysis and mitochondrial function, resulting in the dysfunction of cellular energy metabolism, which could induce intrinsic apoptosis in A549 cells, potentiating synergistic antitumor effects *in vitro* and *in vivo*.

Discussion

Tumor cells are characterized by rapid proliferation, which requires substantial ATP as an energy source (5). Therefore, researchers have begun to consider therapeutic approaches that involve disrupting the energy supply to tumors. However, this strategy has not yet achieved satisfactory therapeutic results. This is possibly because current energy metabolism inhibitors only target partial processes within cellular energy metabolism, while tumor cells such as A549 cells can adaptively regulate other processes to resist external interference and continue to maintain intracellular energy production to support its continued growth and proliferation (35,36). It has been widely recognized that glycolysis, as well as OXPHOS and the TCA cycle within mitochondria, are three critical processes that generate ATP to promote tumor growth, making them key targets in current studies on tumor energy metabolism therapies (37,38). Therefore, it is hypothesized that using a combination of two or more drugs to achieve multifaceted disruption of the energy sources in tumor cells, may prevent or overcome the metabolic self-regulatory capacity of tumor cells (18).

In the present study, two energy metabolism-inhibiting agents (LND and CPI-613) were combined as a novel strategy for the treatment of NSCLC, especially for its main subtype, lung adenocarcinoma (39). Current studies have both highlighted their potential for clinical use and demonstrated their existing limitations. LND, as an energy metabolism inhibitor fostering extensive research attention, has demonstrated its inhibitory effect on glycolysis and OXPHOS in various tumors including NSCLC (13,40,41). However, its efficacy is still not sufficient to meet the clinical treatment requirements. As aforementioned, this may be attributed to the fact that the undisturbed TCA cycle in tumor cells can utilize the products derived from glucose metabolism or other metabolic pathways to maintain energy metabolism (17-22). In addition, CPI-613 is a novel effective inhibitor specifically targeting the TCA cycle (42). When in combination with LND, it is expected to address the limitations of LND, thereby more forcefully

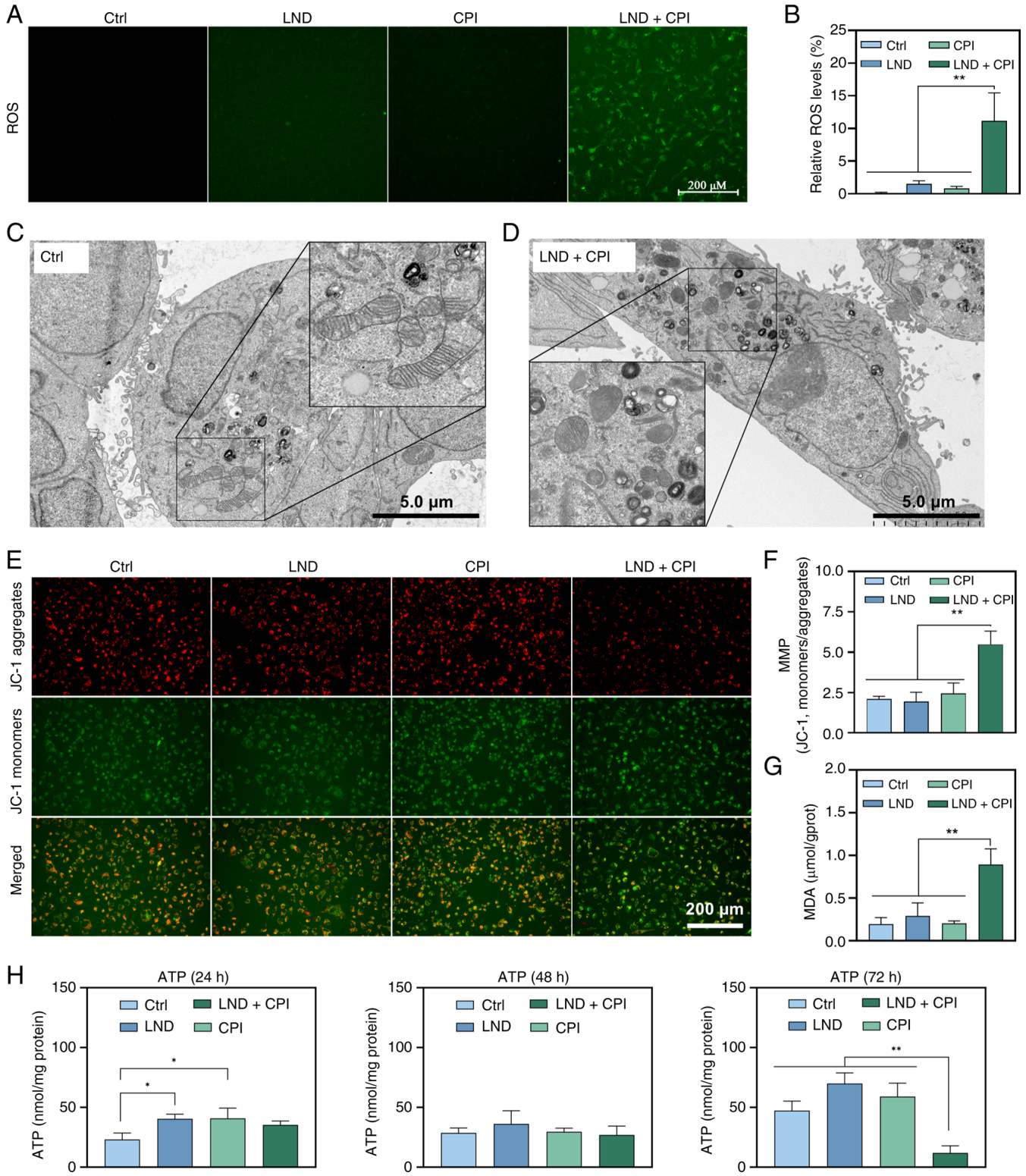

Figure 6. Combination of LND and CPI-613 induces mitochondrial morphology and functional damage in tumor cells. (A) Representative fluorescent images and (B) statistical analysis of ROS content in drug-treated cells (n=3). (C) Transmission electron microscopy of mitochondria in A549 cells before and (D) after co-incubation with LND and CPI-613. (E) Representative micrographs of JC-1-stained A549 cells showing JC-1 aggregates (red fluorescence) and JC-1 monomers (green fluorescence) in mitochondria, and (F) statistical analysis of the MMP calculated by the ratio of JC-1 monomers (green) to aggregates (red) fluorescence (n=3). (G) Measurement of MDA in A549 cells after treated with LND and/ or CPI-613 (n=3). (H) Intracellular ATP concentrations among the four experimental groups after 24, 48 and 72 h treatment with LND and/ or CPI-613 (n=3). *P<0.05 and **P<0.01. ROS, reactive oxygen species; MMP, mitochondrial membrane potential; LND, lonidamine; CPI-613, devimistat; MDA, malondialdehyde.

cutting off the energy metabolism of tumor cells and achieving efficient synergistic treatment. Therefore, at the beginning, the combination effect of LND and CPI-613 was assessed on different NSCLC subtypes. The interaction exhibits a synergistic effect in A549, whereas it was antagonistic in HCC827 and PC9, showing only a partial synergy in H1975. This

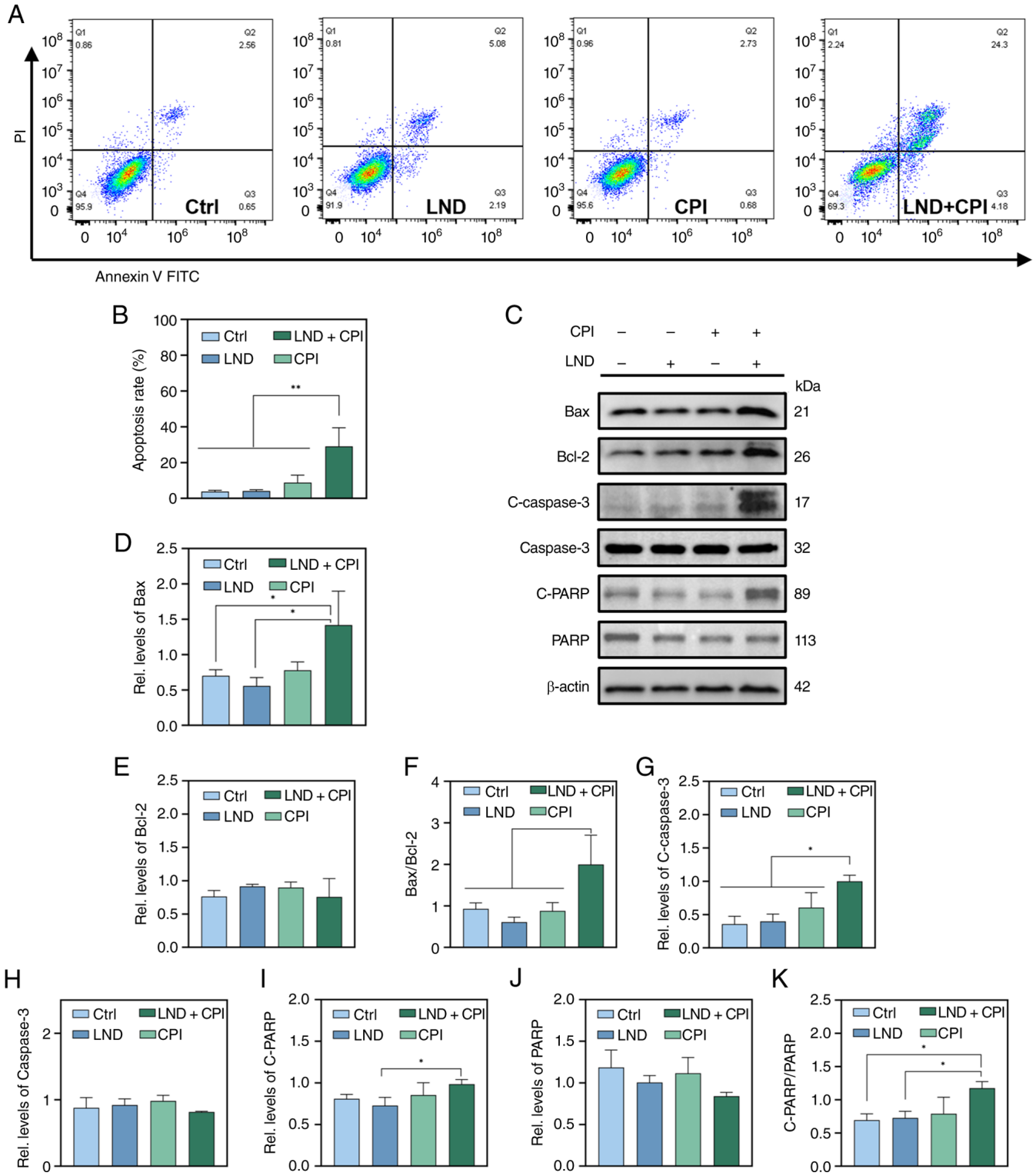

Figure 7. Combination of LND and CPI-613 induces apoptosis in A549 cells. (A) Apoptosis detection of drug-treated cells by flow cytometry. (B) Statistical analysis of apoptotic rates in the four treatment groups. (C) Western blot analysis of apoptotic markers. Original blots are presented in Fig. S7. (D-K) Semi-quantitative analysis of (D) Bax, (E) Bcl-2, (F) the ratio of Bax to Bcl-2, (G) cleaved Caspase 3, (H) Caspase 3, (I) cleaved PARP, (J) PARP and (K) the ratio of cleaved PARP to PARP (n=3). *P<0.05 and **P<0.01. LND, lonidamine; CPI-613, devimistat; PARP, poly (ADP-ribose) polymerase.

inconsistency between different cell lines might originate from distinct genetic mutations and different metabolic preferences across NSCLC subtypes. A549 is KRAS-mutated NSCLC cells, which drives the continuous activation of downstream MAPK and PI3K-AKT-mTOR pathways, leading to a high dependence on glucose metabolism such as aerobic glycolysis to maintain rapid proliferation, thus it is relatively sensitive to energy metabolism inhibitors. By contrast, HCC827, PC9 and H1975 are all EGFR-mutated types (such as 19-del or L858R), and their metabolic regulation is more dependent on the EGFR signaling pathway. Under certain conditions, they can flexibly switch stronger metabolic adaptability (43-46).

The synergistic effect of LND combined with CPI-613 in A549 cells has been demonstrated by the relatively high ZIP synergy score through Synergyfinder analysis, allowing the identification of the optimal dosing regimen for their combination therapy. Specifically, the most effective synergies occurred when LND and CPI-613 were administered in a concentration of ~150 μM. When these concentrations were applied to A549 cells, a notable decrease in cell viability, proliferation and colony-forming capacity was observed. In addition, it was also observed that LND combined with CPI-613 treatment significantly induces apoptosis in A549 cells.

In the xenograft tumor model, the tumor volume and weight in the combination treatment group were significantly smaller than those in both the control and monotherapy groups. TUNEL and Ki-67 staining of tumor tissues also confirmed the highest cytotoxicity and inhibition in the combination group. However, no obvious systemic toxicity was found in the mice after treatment, confirming the safety of the combined treatment regimen. These findings suggested that the combination of LND and CPI-613 induced potent antitumor activity both *in vitro* and *in vivo*, while also maintaining a reliable safety profile.

Previous studies have shown that tumor cells have a high demand for ATP, and extracellular ATP levels in tumors (ATP levels in the tumor mesenchyme) have been found to be 10^3-10^4-fold higher than in normal tissues of the same cellular origin (5,47,48). Inhibiting the generation of ATP in tumor cells can suppress their viability and invasiveness, indicating a promising new strategy for cancer treatment (49,50). In the present study, the combination treatment of LND and CPI-613 resulted in a notable decrease in glycolysis and mitochondrial function, thus resulting in a significant reduction of ATP levels within the cells. On the one hand, it was observed that the combined treatment of LND and CPI-613 could significantly alter the substances related to glycolysis and mitochondrial function at the metabolomics level. On the other hand, damage to the mitochondria of A549 cells further proved that the combination therapy did have an inhibitory effect on cellular energy metabolism, indicating that targeting cellular ATP supply from the perspective of both glycolysis and mitochondrial function could be an effective antitumor therapy. Furthermore, it has been established that this decrease in ATP levels is associated with diminished cell viability and inhibited proliferative capacity (51,52).

Additionally, the impairment of cellular energy metabolism serves as a critical trigger to initiate intrinsic apoptotic pathway. On the one hand, the inherent rapid growth and proliferation characteristics of tumor cells leads to their notable energy requirements, and thus the ATP depletion caused by the combination therapy of LND and CPI-613 will induce a starvation state in tumor cells, making them unable to maintain normal function, and ultimately initiating apoptosis (53,54). On the other hand, the mitochondrial damage occurring during treatment is also an important pathway for inducing cell apoptosis (55). In the present study, the combination of LND and CPI-613, which simultaneously attacked glycolysis, OXPHOS and the TCA cycle, could inhibit the progression of these crucial processes in cellular energy metabolism and induce the accumulation of ROS within A549 cells, as well as an accumulation of the lipid peroxide MDA, which suggests that the combined treatment can induce oxidative damage of mitochondria in A549 cells. Then, the mitochondrial damage, characterized by reduced membrane potential, loss of mitochondrial cristae and alteration of mitochondrial morphology are hypothesized to promote the increase in the Bax/Bcl-2 ratio, a key regulatory node for cell apoptosis (56,57), as well as the release of cytochrome c, thereby activating the apoptotic signaling cascade. The damage, including ATP depletion and mitochondrial perturbations induced by the combination therapy of LND and CPI-613, resulted in the cleavage of caspase 3 and subsequent cleavage of PARP, which collectively enhanced the level of tumor cell apoptosis and strengthened the antitumor therapeutic efficacy (Fig. 7). Therefore, the combined therapy could induce tumor cell apoptosis through ATP depletion-mediated starvation therapy and mitochondrial damage caused by energy metabolism inhibition, which may represent a potential mechanism by which the combined treatment of LND and CPI-613 ultimately culminates in the death of A549 cells.

In summary, the *in vitro* and *in vivo* experiments in the present study provided compelling evidence for the efficacy and safety of the combined treatment of LND and CPI-613. The two agents exerted multifaceted inhibition on cellular energy metabolism by simultaneously disrupting both glycolysis and mitochondrial function, thus synergistically enhancing cytotoxicity and suppressing cell proliferation and inducing apoptosis. These findings suggest that combination therapy involving different energy metabolism inhibitors is a promising strategy for cancer treatment. Furthermore, the strong inhibition of abnormal energy metabolism is expected to enhance the sensitivity of tumors to other treatments (such as chemotherapy, photodynamic therapy and photothermal therapy) (6,7). Additionally, as the immunosuppressive metabolites (such as L-lactic acid) decrease, functional immune cells are activated, which is one of the key factors for the effectiveness of immunotherapy (58).

Nevertheless, there also are some limitations in the present study. Based on the reported clinical data, the maximum serum concentrations of CPI-613 and LND in the human body are only ~80 and ~105 μM, respectively (59,60). However, as in other preclinical studies involving CPI-613 or LND (41,61-63), in order to achieve a significant tumor suppression effect, very high drug concentrations had to be used in the present study. Furthermore, due to the significant adverse reactions and unexpected deaths caused by systemic intravenous administration of LND and CPI-613 in mice, the present study was forced to adopt the intratumoral injection to ensure successful drug intervention and observe the direct antitumor effect of the combined treatment, which is also an obstacle to achieving clinical application. To address these limitations, further research will focus on chemically modifying the drugs or developing efficient delivery systems. In addition, increased ROS accumulation, elevated MDA levels and abnormal mitochondrial morphology observed in the present study suggest that ferroptosis cannot be excluded and warrants investigation in future research. In the present study, Ki-67 and TUNEL staining within tumor tissues verified the antiproliferative and pro-apoptotic effects induced

by combined treatment. Nevertheless, these indicators cannot serve as direct pharmacodynamic evidence of metabolic target engagement *in vivo*, which remains an obvious limitation of the current research. Further targeted detection *in vivo* will be implemented in future studies to support clinical applicability.

Acknowledgements

The authors would like to thank Miss Yijing Long and Miss Fei Fu (Core Facility of West China Hospital Sichuan University) for providing the corresponding instruments and technical support.

Funding

The present study was supported by Sichuan Science and Technology Program (grant no. 2025ZNSFSC0246), the National Natural Science Foundation of China (grant nos. 22175144 and 22208269), the science and Technology Plan Project of Luzhou (grant no. 2025JYJ038), the Joint Project between Luzhou Municipal People's Government and Southwest Medical University (grant nos. 2021LZXNYD-J17, 2024LZXNYDJ079 and 2023LZXNYDJ008), the Foundation of Southwest Medical university (grant no. 2021ZKZD012) and the College Students Innovation and Entrepreneurship Training Program of Southwest Medical University (grant no. 2024451).

Availability of data and materials

The data generated in the present study may be found in the OMIX, China National Center for Bioinformation/Beijing Institute of Genomics, Chinese Academy of Sciences under accession number OMIX017768 or at the following URL: https://ngdc.cncb.ac.cn/omix/release/OMIX017768. The data generated in the present study are included in the figures and/or tables of this article.

Authors' contributions

YH, QF and SG conceived and designed the experiments. XB, YY, YL, PJ, XH, YZ and YD performed the experiments. XB, YY, YL, XY, MZ, HX, YH, QF and SG analyzed the data. XB, YY, QF and SG wrote the manuscript. XB, YY, YL, YH, QF and SG confirm the authenticity of all the raw data. All authors read and approved the final version of the manuscript.

Ethics approval and consent to participate

In vivo animal experiments were conducted following approval by the Instructional Animal Care and Use Committee of Southwest Medical University (approval no. 20210223-079, date: 25 February 2021; Luzhou, China), and all procedures adhered to National Research Council's Guide for the Care and Use of Laboratory Animals.

Patient consent for publication

Not applicable.

Competing interests

The authors declare that they have no competing interests.

References

1. Bray F, Laversanne M, Sung H, Ferlay J, Siegel RL, Soerjomataram I and Jemal A: Global cancer statistics 2022: GLOBOCAN estimates of incidence and mortality worldwide for 36 cancers in 185 countries. CA Cancer J Clin 74: 229-263, 2024.
2. Li C, Lei S, Ding L, Xu Y, Wu X, Wang H, Zhang Z, Gao T, Zhang Y and Li L: Global burden and trends of lung cancer incidence and mortality. Chin Med J (Engl) 136: 1583-1590, 2023.
3. Zappa C and Mousa SA: Non-small cell lung cancer: Current treatment and future advances. Transl Lung Cancer Res 5: 288-300, 2016.
4. Lyu Y, Yang J, Cheng L, Li Z and Zheng J: Benzo(a)pyrene-induced mitochondrial respiration and glycolysis disturbance in human neuroblastoma cells. J Toxicol Sci 48: 87-97, 2023.
5. Kim SY: Targeting cancer energy metabolism: A potential systemic cure for cancer. Arch Pharm Res 42: 140-149, 2019.
6. Ding XL, Liu MD, Cheng Q, Guo WH, Niu MT, Huang QX, Zeng X and Zhang XZ: Multifunctional liquid metal-based nanoparticles with glycolysis and mitochondrial metabolism inhibition for tumor photothermal therapy. Biomaterials 281: 121369, 2022.
7. Pateras IS, Williams C, Gianniou DD, Margetis AT, Avgeris M, Rousakis P, Legaki AI, Mirtschink P, Zhang W, Panoutsopoulou K, *et al*: Short term starvation potentiates the efficacy of chemotherapy in triple negative breast cancer via metabolic reprogramming. J Transl Med 21: 169, 2023.
8. Nath K, Guo L, Nancolas B, Nelson DS, Shestov AA, Lee SC, Roman J, Zhou R, Leeper DB, Halestrap AP, *et al*: Mechanism of antineoplastic activity of lonidamine. Biochim Biophys Acta 1866: 151-162, 2016.
9. Mansi JL, de Graeff A, Newell DR, Glaholm J, Button D, Leach MO, Payne G and Smith IE: A phase II clinical and pharmacokinetic study of Lonidamine in patients with advanced breast cancer. Br J Cancer 64: 593-597, 1991.
10. Meijer TWH, Peeters WJM, Dubois LJ, van Gisbergen MW, Biemans R, Venhuizen JH, Span PN and Bussink J: Targeting glucose and glutamine metabolism combined with radiation therapy in non-small cell lung cancer. Lung Cancer 126: 32-40, 2018.
11. Chen E, Wang T, Zhang J, Zhou X, Niu Y, Liu F, Zhong Y, Huang D and Chen W: Mitochondrial targeting and pH-responsive nanogels for Co-delivery of lonidamine and paclitaxel to conquer drug resistance. Front Bioeng Biotechnol 9: 787320, 2021.
12. Cervantes-Madrid D, Romero Y and Dueñas-González A: Reviving lonidamine and 6-Diazo-5-oxo-L-norleucine to be used in combination for metabolic cancer therapy. Biomed Res Int 2015: 690492, 2015.
13. Fan T, Shen L, Huang Y, Wang X, Zhao L, Zhong R, Wang P and Sun G: Lonidamine increases the cytotoxic effect of 1-[(4-Amino-2-methyl-5-pyrimidinyl) methyl]-3-(2-chloroethyl)-3-nitrosourea via energy inhibition, disrupting redox homeostasis, and downregulating MGMT expression in human lung cancer cell line. ACS Omega 9: 36134-36147, 2024.
14. Zhou Y, Shi J, Zhang M, Yang H and Fei J: The interventional effects and mechanisms of Lonidamine in combination with apigenin on colorectal cancer. Curr Issues Mol Biol 47: 825, 2025.
15. Orlovskiy S, Gupta PK, Arias-Mendoza F, Singh DK, Nova S, Nelson DS, Narayan V, Koch CJ, Hardy M, You M, *et al*: Enhancing radiation therapy response in prostate cancer through metabolic modulation by Mito-lonidamine: A 1H and 31P magnetic resonance spectroscopy study. Int J Mol Sci 26: 509, 2025.
16. Xiang C, Ding Q, Jiang T, Liu Y, Li C, Yang X, Jia J, Xiang J, Wang Y, Zhou H, *et al*: Reprogrammed glycolysis-induced augmentation of NIR-II excited photodynamic/photothermal therapy. Biomaterials 320: 123235, 2025.
17. Martínez-Reyes I and Chandel NS: Cancer metabolism: Looking forward. Nat Rev Cancer 21: 669-680, 2021.

18. Stine ZE, Schug ZT, Salvino JM and Dang CV: Targeting cancer metabolism in the era of precision oncology. Nat Rev Drug Discov 21: 141-162, 2022.
19. Eniafe J and Jiang S: The functional roles of TCA cycle metabolites in cancer. Oncogene 40: 3351-3363, 2021.
20. Wu J, Liu N, Chen J, Tao Q, Li Q, Li J, Chen X and Peng C: The tricarboxylic acid cycle metabolites for cancer: Friend or enemy. Research (Wash D C) 7: 0351, 2024.
21. Kenny TC and Birsoy K: Mitochondria and cancer. Cold Spring Harb Perspect Med 14: a041534, 2024.
22. Cai L, Hammond NG, Tasdogan A, Alsamraae M, Yang C, Cameron RB, Quan P, Solmonson A, Gu W, Pachnis P, *et al*: High glucose contribution to the TCA cycle is a feature of aggressive Non-Small cell lung cancer in patients. Cancer Discov 15: 702-716, 2025.
23. Anderson NM, Mucka P, Kern JG and Feng H: The emerging role and targetability of the TCA cycle in cancer metabolism. Protein Cell 9: 216-237, 2018.
24. Yang J, Chen F, Fu Z, Yang F, Saba NF and Teng Y: Blocking the TCA cycle in cancer cells potentiates CD36+ T-cell-Mediated antitumor immunity by suppressing ER Stress-associated THBS2 signaling. Cancer Res 85: 2014-2026, 2025.
25. Neitzel C, Demuth P, Wittmann S and Fahrer J: Targeting altered energy metabolism in colorectal cancer: Oncogenic reprogramming, the central role of the TCA cycle and therapeutic opportunities. Cancers 12: 1731, 2020.
26. Stuart SD, Schauble A, Gupta S, Kennedy AD, Keppler BR, Bingham PM and Zachar Z: A strategically designed small molecule attacks alpha-ketoglutarate dehydrogenase in tumor cells through a redox process. Cancer Metab 2: 4, 2014.
27. Guardado Rivas MO, Stuart SD, Thach D, Dahan M, Shorr R, Zachar Z and Bingham PM: Evidence for a novel, effective approach to targeting carcinoma catabolism exploiting the first-in-class, anti-cancer mitochondrial drug, CPI-613. PLoS One 17: e0269620, 2022.
28. Lang L, Wang F, Ding Z, Zhao X, Loveless R, Xie J, Shay C, Qiu P, Ke Y, Saba NF and Teng Y: Blockade of glutamine-dependent cell survival augments antitumor efficacy of CPI-613 in head and neck cancer. J Exp Clin Cancer Res 40: 393, 2021.
29. Udumula MP, Rashid F, Singh H, Pardee T, Luther S, Bhardwaj T, Anjaly K, Piloni S, Hijaz M, Gogoi R, *et al*: Targeting mitochondrial metabolism with CPI-613 in chemoresistant ovarian tumors. J Ovarian Res 17: 226, 2024.
30. Lycan TW, Pardee TS, Petty WJ, Bonomi M, Alistar A, Lamar ZS, Isom S, Chan MD, Miller AA and Ruiz J: A Phase II clinical trial of CPI-613 in patients with relapsed or refractory small cell lung carcinoma. PLoS One 11: e0164244, 2016.
31. Chou TC: Drug combination studies and their synergy quantification using the Chou-Talalay method. Cancer Res 70: 440-446, 2010.
32. Jonsson P, Gullberg J, Nordström A, Kusano M, Kowalczyk M, Sjöström M and Moritz T: A strategy for identifying differences in large series of metabolomic samples analyzed by GC/MS. Anal Chem 76: 1738-1745, 2004.
33. Yankovskaya V, Horsefield R, Törnroth S, Luna-Chavez C, Miyoshi H, Léger C, Byrne B, Cecchini G and Iwata S: Architecture of succinate dehydrogenase and reactive oxygen species generation. Science 299: 700-704, 2003.
34. Qi W, Lu C, Huang H, Zhang W, Song S and Liu B: (+)-Usnic acid induces ROS-dependent apoptosis via inhibition of mitochondria respiratory Chain complexes and Nrf2 expression in lung squamous cell carcinoma. Int J Mol Sci 21: 876, 2020.
35. Halma MTJ, Tuszynski JA and Marik PE: Cancer metabolism as a therapeutic target and review of interventions. Nutrients 15: 4245, 2023.
36. Tufail M, Jiang CH and Li N: Altered metabolism in cancer: Insights into energy pathways and therapeutic targets. Mol Cancer 23: 203, 2024.
37. Payen VL, Mina E, Van Hée VF, Porporato PE and Sonveaux P: Monocarboxylate transporters in cancer. Mol Metab 33: 48-66, 2020.
38. Liu Y, Sun Y, Guo Y, Shi X, Chen X, Feng W, Wu LL, Zhang J, Yu S, Wang Y and Shi Y: An overview: The diversified role of mitochondria in cancer metabolism. Int J Biol Sci 19: 897-915, 2023.
39. Chen H, Jiang T, Yang Y, Cai G, Jiang Y and Ouyang W: Exploring the carcinogenic potential of bisphenol A in lung adenocarcinoma: Molecular mechanisms, key gene insights, and immune microenvironment impacts. Front Immunol 16: 1647807, 2025.
40. Shang C, Hou Y, Meng T, Shi M and Cui G: The anticancer activity of indazole compounds: A mini review. Curr Top Med Chem 21: 363-376, 2021.
41. Cheng G, Zhang Q, Pan J, Lee Y, Ouari O, Hardy M, Zielonka M, Myers CR, Zielonka J, Weh K, *et al*: Targeting lonidamine to mitochondria mitigates lung tumorigenesis and brain metastasis. Nat Commun 10: 2205, 2019.
42. Reddy VB, Boteju L, Boteju A, Shen L, Kassahun K, Reddy N, Sheldon A, Luther S and Hu K: In vitro and in vivo metabolism of a novel antimitochondrial cancer metabolism agent, CPI-613, in rat and human. Drug Metab Dispos 50: 361-373, 2022.
43. Saliakoura M, Rossi Sebastiano M, Pozzato C, Heidel FH, Schnöder TM, Savic Prince S, Bubendorf L, Pinton P, A Schmid R, Baumgartner J, *et al*: PLCγ1 suppression promotes the adaptation of KRAS-mutant lung adenocarcinomas to hypoxia. Nat Cell Biol 22: 1382-1395, 2020.
44. Cao HJ, Zhou W, Xian XL, Sun SJ, Ding PJ, Tian CY, Tian FL, Jiang CH, Fu TT, Zhao S and Dai JY: A Mixture of baicalein, wogonin, and oroxylin-a inhibits EMT in the A549 cell line via the PI3K/AKT-TWIST1-glycolysis pathway. Front Pharmacol 12: 821485, 2022.
45. Vojnic M, Kubota D, Kurzatkowski C, Offin M, Suzawa K, Benayed R, Schoenfeld AJ, Plodkowski AJ, Poirier JT, Rudin CM, *et al*: Acquired BRAF rearrangements induce secondary resistance to EGFR therapy in EGFR-Mutated lung cancers. J Thorac Oncol 14: 802-815, 2019.
46. Joshi H and Sheikh MS: Cell death, molecular targeted therapies, and metabolic reprogramming in EGFR-Mutant lung cancer. Cancers (Basel) 17: 2791, 2025.
47. Qian Y, Wang X, Li Y, Cao Y and Chen X: Extracellular ATP a new player in cancer metabolism: NSCLC cells Internalize ATP in vitro and in vivo using multiple endocytic mechanisms. Mol Cancer Res 14: 1087-1096, 2016.
48. De Marchi E, Orioli E, Pegoraro A, Adinolfi E and Di Virgilio F: Detection of extracellular ATP in the tumor microenvironment, using the pmeLUC biosensor. Methods Mol Biol 2041: 183-195, 2020.
49. Wang TA, Xian SL, Guo XY, Zhang XD and Lu YF: Combined 18F-FDG PET/CT imaging and a gastric orthotopic xenograft model in nude mice are used to evaluate the efficacy of glycolysis-targeted therapy. Oncol Rep 39: 271-279, 2018.
50. Vultaggio-Poma V, Sarti AC and Di Virgilio F: Extracellular ATP: A feasible target for cancer therapy. Cells 9: 2496, 2020.
51. Ye S, Zhou HB, Chen Y, Li KQ, Jiang SS and Hao K: Crizotinib changes the metabolic pattern and inhibits ATP production in A549 non-small cell lung cancer cells. Oncol Lett 21: 61, 2021.
52. Wei J, Lei G, Chen Q, Huang W, Ning H, Yang M, Dong J, Hu L, Peng S, Gong H, *et al*: Casticin inhibits proliferation of Non-small cell lung cancer cells through regulating reprogramming of glucose metabolism. Phytomedicine 136: 156278, 2025.
53. Fu Z, Du H, Meng S, Yao M, Zhao P, Li X, Zheng X, Yuan Z, Yang H, Cai K and Dai L: Tumor-targeted dual-starvation therapy based on redox-responsive micelle nanosystem with co-loaded LND and BPTES. Mater Today Bio 16: 100449, 2022.
54. Wu Y, Zhang Z, Ren M, Chen Y, Zhang J, Li J, Gao F, Bao Y, Huang Y, Yang X, *et al*: Metformin induces apoptosis and ferroptosis of ovarian cancer cells under energy stress conditions. Cells 14: 213, 2025.
55. Ma Z, Han H and Zhao Y: Mitochondrial dysfunction-targeted nanosystems for precise tumor therapeutics. Biomaterials 293: 121947, 2023.
56. Ouyang W, Zhu C, Li Y, Huang H, Li F and Ling L: Assessing the neurotoxic risks of triethyl citrate in daily environmental exposure using network toxicology and molecular docking. Ecotoxicol Environ Saf 297: 118225, 2025.
57. Ouyang W, Deng Z, Li Y, Chi W, Huang Z, Zhan C, Li M, Wang D, Li F, Liu Y and Ling L: Traditional Chinese medicine in cerebral infarction: Integrative strategies and future directions. Phytomedicine 143: 156841, 2025.
58. Ouyang W, Peng Q, Lai Z, Huang H, Huang Z, Xie X, Lin R, Wang Z, Yao H and Yu Y: Synergistic role of activated CD4+ memory T cells and CXCL13 in augmenting cancer immunotherapy efficacy. Heliyon 10: e27151, 2024.
59. Philip PA, Sahai V, Bahary N, Mahipal A, Kasi A, Rocha Lima CMS, Alistar AT, Oberstein PE, Golan T, Metges JP, *et al*: Devimistat (cpi-613) with modified fluorouarcil, oxaliplatin, irinotecan, and leucovorin (FFX) versus FFX for patients with metastatic adenocarcinoma of the pancreas: The phase III avenger 500 study. J Clin Oncol 42: 3692-3701, 2024.

60. Di Cosimo S, Ferretti G, Papaldo P, Carlini P, Fabi A and Cognetti F: Lonidamine: Efficacy and safety in clinical trials for the treatment of solid tumors. Drugs Today (Barc) 39: 157-174, 2003.
61. Wang H, Zhang Y, Jiang Y, Xiang R, Gong H, Gong Y, Xu H, Ma Z, Xie Y, Zhu Y, *et al*: The function and mechanism of clinical trial agent CPI-613 in multiple myeloma. Biochem Pharmacol 232: 116717, 2025.
62. Gao L, Xu Z, Huang Z, Tang Y, Yang D, Huang J, He L, Liu M, Chen Z and Teng Y: CPI-613 rewires lipid metabolism to enhance pancreatic cancer apoptosis via the AMPK-ACC signaling. J Exp Clin Cancer Res 39: 73, 2020.
63. Wang Q, Li S, Xu C, Hua A, Wang C, Xiong Y, Deng Q, Chen X, Yang T, Wan J, *et al*: A novel lonidamine derivative targeting mitochondria to eliminate cancer stem cells by blocking glutamine metabolism. Pharmacol Res 190: 106740, 2023.